Articles

Structures and Magnetic Properties of Ternary Lithium Oxides LiRO_2 (R = Rare Earths)

Yuta Hashimoto, Makoto Wakeshima, Kazuyuki Matsuhira, and Yukio Hinatsu*

Division of Chemistry, Graduate School of Science, Hokkaido University, Sapporo 060-0810, Japan

Yoshinobu Ishii

Japan Atomic Energy Research Institute, Tokai-mura, Ibaraki 319-1195, Japan

Received August 9, 2001. Revised Manuscript Received February 11, 2002

Crystal structures and magnetic properties of ternary lithium oxides LiRO_2 (R = rare earths) are investigated. Their crystal structures are grouped into four type structures (α, β, γ, δ-types). From their low-temperature X-ray diffraction and differential thermal analysis measurements, the LiRO_2 compounds with R = Dy, Ho, Y, and Er transform from the monoclinic β-type (low-temperature phase) to the tetragonal α-type structures (high-temperature phase) at 475, 360, 325, and 200 K, respectively. Through their magnetic susceptibility and specific heat measurements, the Sm, Gd, Dy, and Er compounds show antiferromagnetic transitions at 1.9, 2.5, 3.0, and 4.2 K, respectively. Both $LiNdO_2$ and $LiYbO_2$ show magnetic anomaly below 1.8 K.

Introduction

Syntheses and crystal structures of ternary lithium-rare earth oxides LiRO_2 (R = rare earths) have been investigated since the R = Er, Yb, Lu compounds were first synthesized by Hoppe.[1] Their crystal structures have been grouped into four types (α, β, γ, δ-type) depending on rare-earth ionic radius. The α-LiRO_2 compounds, which contain small rare earths (R = Sc, Y, Lu, Yb, Tm, Er), crystallize in a tetragonal structure with the space group $I4_1/amd$.[2] The β-LiRO_2 compounds containing medium-size rare earths (R = Y, Tb, Ho, Dy) have a lower symmetric monoclinic structure (space group $P2_1/c$) as compared with the α-type structure.[3] In the α- and β-type structures, the R ions are coordinated octahedrally by six oxide ions and each RO_6 octahedron shares four edges and four corners with the surrounding RO_6 octahedra. The approximate relations between the cell vectors of the tetragonal α-type and the distorted monoclinic β-type are described by,[3]

$$\mathbf{a}_m \sim 1/2(\mathbf{a}_t + \mathbf{b}_t + \mathbf{c}_t); \quad \mathbf{b}_m \sim \mathbf{a}_t - \mathbf{b}_t; \quad \mathbf{c}_m \sim 1/2(\mathbf{a}_t + \mathbf{b}_t - \mathbf{c}_t) \quad (1)$$

where the monoclinic cell vectors $\mathbf{a}_m$ and $\mathbf{c}_m$ have nearly the same length, and the angle β is nearly equal to 120°.

The γ-LiRO_2 (R = Tb, Eu, Gd, Sm) compounds with an orthorhombic structure (space group: $Pbnm$) are formed by the connection of one edge-sharing and two corner-sharing RO_6 octahedra.[4] The δ-LiRO_2 compounds containing large rare earths (R = La ∼ Nd, Sm, Eu) crystallize in a monoclinic structure (space group: $P2_1/c$), which consists of two different types of RO_7 decahedra coordinated by seven oxide ions.[5] The crystal structures of a series of LiRO_2 were summarized in ref 6.

Faucher et al. found that a Eu^{3+}-doped $LiYO_2$ compound showed the structural transition from β-type to α-type at 342 K during heating.[7] Waintal and Gondrand reported the effect of pressure on the structure type of some compounds.[6] The spectroscopic properties on LiRO_2 were studied by several researchers.[8−10] For the magnetic properties, only the paramagnetic behavior of δ-$LiCeO_2$ above liquid-He temperature was reported.[11]

In this study, we have paid attention to the structural and magnetic properties of the ternary lithium oxides, LiRO_2. Some interesting structural transitions and magnetic anomalies have been found through powder X-ray and neutron diffraction, magnetic susceptibility, differential thermal analysis (DTA), and specific heat measurements, and their results are discussed here.

* To whom correspondence should be addressed.

(1) Hoppe, R. *Angew. Chem.* **1959**, *71*, 457.
(2) Glaum, H.; Voigt, S.; Hoppe, R. *Z. Anorg. Allg. Chem.* **1991**, *598/599*, 129.
(3) Bertaut, F.; Gondrand, M. *C. R. Acad. Sci.* **1962**, *255*, 1135.
(4) Gondrand, M.; Bertaut, F. *Bull. Soc. Fr. Minéral. Cristallogr.* **1963**, *86*, 301.
(5) Bärnighausen, H. *Acta Crystallogr.* **1965**, *19*, 1048.
(6) Waintal, M.; Gondrand, M. *Mater. Res. Bull.* **1967**, *2*, 889.
(7) Faucher, M. D.; Sciau, P.; Kiat, J.-M.; Alves, M.-G.; Bouree, F. *J. Solid State Chem.* **1998**, *137*, 242.
(8) Blasse, G. *J. Chem. Phys.* **1966**, *45*, 2356.
(9) Blasse, G.; Bril, A. *J. Chem. Phys.* **1966**, *45*, 3327.
(10) Blasse, G.; Roos, A.; Van der Steen, A. C. *J. Solid State Chem.* **1978**, *24*, 233.
(11) Lueken, H.; Hannibal, P.; Stamm, U. *Z. Anorg. Allg. Chem.* **1984**, *516*, 107.

10.1021/cm010728u CCC: $22.00
Published on Web 06/28/2002

Experimental Section

Samples were prepared by the solid-state reaction. As starting materials, R_2O_3 (R = Sc, Y, Pr, Nd, Sm−Lu) and Li_2CO_3 were used. These reagents were weighed in the Li/R = 1.5 metal ratios to prevent loss of lithium from evaporation, and ground in an agate mortar. The mixtures were pelletized and heated in air (except for the R = Pr, Eu, Tb compounds) at 1173 K for 12−48 h with some addition of Li_2CO_3 and several regrindings. For the R = Pr, Eu, Tb compounds, the samples were heated in an Ar + 7% H_2 atmosphere at 1173 K.

Powder X-ray diffraction profiles were measured using a Rigaku Multi-Flex diffractometer with CuKα radiation equipped with a curved graphite monochromator. The data were collected by step scanning in the angle range $10° \le 2\theta \le 120°$ at a 2θ step size of 0.04°. For $LiErO_2$, powder neutron diffraction measurements at 150 and 250 K were carried out with a high-resolution powder diffractometer (HRPD) in the JRR-3M reactor (Japan Atomic Energy Research Institute), with a Ge(331) monochromator (λ = 1.823 Å).

The temperature dependence of the magnetic susceptibility was measured with a SQUID magnetometer (Quantum Design, MPMS) under both zero-field-cooled conditions (ZFC) and field-cooled conditions (FC). The former was measured on heating the sample to 300 K under the applied magnetic field of 0.1 T after zero-field cooling to 1.8 K. The latter was measured upon cooling the sample from 10 to 1.8 K under 0.1 T.

The specific heats were measured using a relaxation technique applied by a specific heat measuring system (Quantum Design, PPMS) in the temperature range $1.8 \le T \le 400$ K. The sample in the form of a thin plate was mounted on a sample holder with Apiezon for better thermal contact. For $LiErO_2$, to prevent a separation of the sample from a sample holder near its structural transition temperature, a thin plate of $LiErO_2$ was lapped in a copper film, and then mounted on the sample holder with Apiezon. DTA measurement was carried out in the temperature range $300 \le T \le 550$ K using TG-DTA2000S (MAC Science Co., Ltd).

Results and Discussion

Crystal Structures. All the LiRO$_2$ compounds except for δ-LiRO$_2$ were obtained as a single phase. For δ-LiRO$_2$, small amounts of unknown impurities were observed. From the powder X-ray diffraction patterns, their crystal structures are grouped into four following structural types:

R = Er ∼ Lu, Sc: α-type (space group: $I4_1/amd$)

R = Tb ∼ Dy, Y: β-type (space group: $P2_1/c$)

R = Eu ∼ Tb: γ-type (space group: $Pbnm$)

R = Pr, Nd, Sm: δ-type (space group: $P2_1/c$)

The $LiTbO_2$ compound was previously reported to crystallize in a γ-type structure. We are the first group who prepared $LiTbO_2$ compound with a β-type structure by heating in an Ar + 7% H_2 atmosphere at 1173 K for 12 h.

We have performed the Rietveld analysis with the program RIETAN-97[12] for the diffraction profiles. Figure 1 shows the typical powder X-ray diffraction patterns for the four types of compounds, α-$LiErO_2$, β-$LiHoO_2$, γ-$LiTbO_2$, and δ-$LiNdO_2$. The X-ray diffraction pattern of the β-type structure has splitting diffraction peaks compared to those of the α-type structure, because the

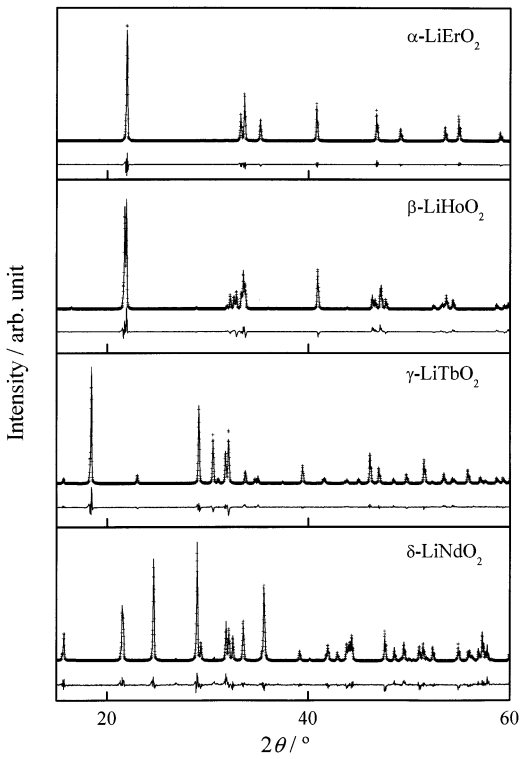

Figure 1. Powder X-ray diffraction patterns for α-$LiErO_2$, β-$LiHoO_2$, γ-$LiTbO_2$, and δ-$LiNdO_2$.

Table 1. Lattice Parameters and Reliability Factors for LiRO$_2$ Determined by X-Ray Diffraction Measurements at Room Temperature

compounds	a (Å)	b (Å)	c (Å)	β (°)	R_{wp}[a]	R_I[b]
α-$LiScO_2$	4.1874(1)		9.3198(1)		18.99	11.24
α-$LiLuO_2$	4.3793(1)		9.9847(1)		14.70	3.69
α-$LiYbO_2$	4.3877(1)		10.0555(1)		12.09	2.58
α-$LiTmO_2$	4.4100(1)		10.1194(1)		11.56	3.31
α-$LiErO_2$	4.4318(1)		10.2234(1)		13.12	3.46
β-$LiYO_2$	6.1218(2)	6.1948(1)	6.2017(2)	118.705(2)	14.88	3.63
β-$LiHoO_2$	6.1313(2)	6.1822(1)	6.2200(2)	118.745(2)	19.13	9.40
β-$LiDyO_2$	6.1912(2)	6.1721(2)	6.2948(2)	119.153(2)	24.08	8.40
β-$LiTbO_2$	6.2536(6)	6.1716(3)	6.3661(5)	119.486(6)	15.76	4.34
γ-$LiTbO_2$	11.2593(2)	3.4256(1)	5.3090(1)		14.46	6.35
γ-$LiGdO_2$	11.3567(4)	3.4489(1)	5.3312(2)		27.19	11.92
γ-$LiEuO_2$	11.4059(2)	3.4721(1)	5.3372(1)		22.78	8.43
δ-$LiSmO_2$	5.7051(1)	6.0211(1)	5.6492(1)	103.038(1)	23.52	12.01
δ-$LiNdO_2$	5.7661(1)	6.0211(1)	5.7162(1)	102.923(1)	25.63	9.75
δ-$LiPrO_2$	5.7968(1)	6.1210(1)	5.7535(1)	102.815(2)	27.94	13.27

[a] $R_{wp} = |\sum w(|F(o)| - |F(c)|)^2/\sum w|F(o)|^2|^{1/2}$. [b] $R_I = \sum|I_k(o) - I_k(c)|/\sum I_k(o)$.

β-type structure is distorted from the α-type structure. Table 1 lists the lattice parameters and reliability factors for the LiRO$_2$ compounds prepared in this study. For the α-, γ-, and δ-type compounds, the lattice parameters decrease with the decreasing ionic radius of the R^{3+} ion. On the contrary, the a and c parameters of β-type compounds increase and the b parameters decrease with decreasing the ionic radius of the R^{3+} ion. Large reliability factors may indicate the inclusion of some impurities.

Figure 2a shows the powder X-ray diffraction patterns for $LiErO_2$ measured at 15, 200, 210, and 300 K. The diffraction pattern of the α-type structure was observed at 210 and 300 K, while that of the β-type structure was observed at 15 and 200 K. These results indicate that $LiErO_2$ transforms from the β-type structure to the α-type structure at a temperature between 200 and 210

(12) Izumi, F.; Ikeda, T. *Mater. Sci. Forum* **2000**, *321*, 198.

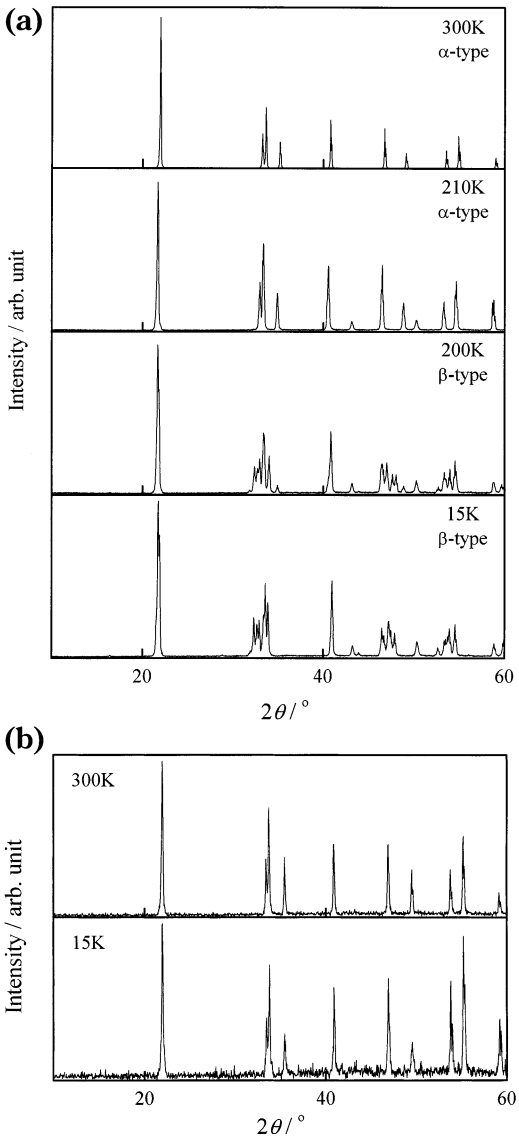

Figure 2. Powder X-ray diffraction patterns for (a) $LiErO_2$ at 15, 200, 210, and 300 K and (b) α-$LiTmO_2$ at 15 and 300 K.

K. Low-temperature X-ray diffraction measurements for $LiTmO_2$ were also performed in the temperature range of 15−300 K and the diffraction patterns at 15 and 300 K are shown in Figure 2b. They show the same diffraction pattern for the α-type structure, indicating that $LiTmO_2$ has no structural transition from α-type to *β*-type structure in this temperature range.

To determine accurately the positional parameters of the lithium and oxygen sites for the α- and *β*-$LiErO_2$, neutron diffraction measurements for the $LiErO_2$ were performed at 250 and 150 K. The neutron diffraction profiles at 150 and 250 K (Figure 3a,b, respectively) are indexed in the *β*-type and α-type structures, respectively. The refined lattice parameters and positional parameters are listed in Table 2. The cell volume at 150 K becomes about 1% larger than that at 250 K by the structural transition. The Li−O and Er−O interatomic distances are calculated from the refined parameters and they are listed in Table 3. The Er−O distances in the ErO_6 octahedron are almost equidistant (2.2−2.3 Å) in both of the α- and *β*-type structures. On the other hand, the LiO_6 polyhedron in the *β*-type structure has

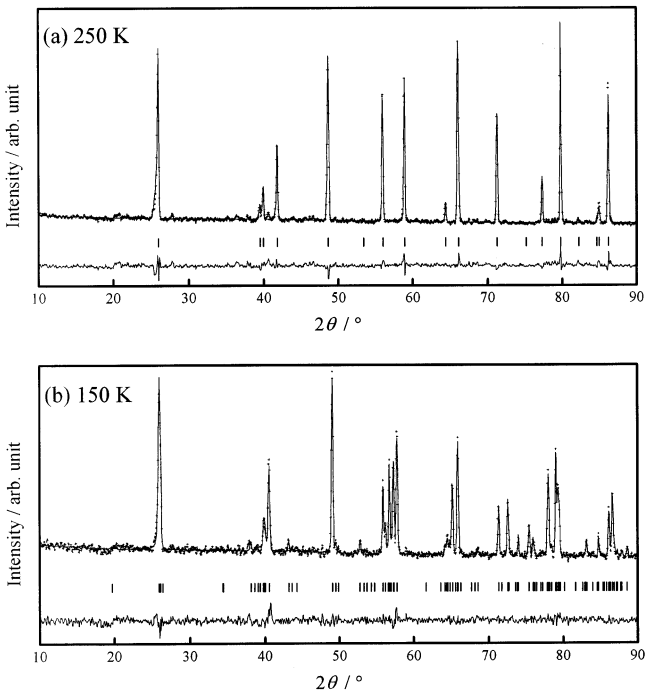

Figure 3. Powder neutron diffraction patterns for $LiErO_2$ at (a) 150 and (b) 250 K.

Table 2. Cell Parameters and Positional Parameters of $LiErO_2$ Obtained from Refinement of Neutron Powder Diffraction Patterns at 150 and 250 K

150 K (Monoclinic *β*-Type) Space Group *P*21/*c*,
$Z = 4$, $a = 6.0761(6)$ Å, $b = 6.1617(4)$ Å, $c = 6.1546(6)$ Å,
$\beta = 118.479(4)°$, $V = 202.54(3)$ Å^3, $R_{wp} = 8.20\%$, $R_I = 4.43\%$

atom	site	*x*	*y*	*z*	*B*/Å^2
Li	4e	0.284(9)	0.649(9)	0.052(9)	0.69(18)
Er	4e	0.2376(6)	0.1311(5)	−0.0149(5)	0.29(5)
O(1)	4e	0.4555(6)	0.3924(6)	0.2617(6)	0.03(6)
O(2)	4e	−0.0079(7)	0.1645(5)	0.1672(7)	0.17(6)

250 K (Tetragonal α-Type) Space Group $I4_1/amd$,
$Z = 4$, $a = 4.4291(2)$ Å, $c = 10.2210(5)$ Å, $V = 200.50(2)$ Å^3
$R_{wp} = 7.42\%$, $R_I = 5.46\%$

atom	site	*x*	*y*	*z*	*B*/Å^2
Li	4a	0	0	1/2	0.99(11)
Er	4b	0	0	0	0.10(6)
O	8e	0	0	0.2234(1)	0.84(6)

Table 3. Interatomic Distances for $LiErO_2$ Determined by Neutron Diffraction Measurements at 150 and 250 K

Distance/Å			
150 K (Monoclinic *β*-Type)			
Li−O(1) ×1	2.00(1)	Er−O(1) ×1	2.212(4)
Li−O(1) ×1	2.08(1)	Er−O(1) ×1	2.302(4)
Li−O(1) ×1	3.04(2)	Er−O(1) ×1	2.323(7)
Li−O(2) ×1	1.94(1)	Er−O(2) ×1	2.203(5)
Li−O(2) ×1	2.91(1)	Er−O(2) ×1	2.212(4)
Li−O(2) ×1	2.92(2)	Er−O(2) ×1	2.262(7)
250 K (Tetragonal α-Type)			
Li−O ×4	2.231(1)	Er−O ×4	2.231(1)
Li−O ×2	2.823(1)	Er−O ×2	2.287(1)

three short Li−O distances (∼2 Å) and three long Li−O distances (∼3 Å), while the Li−O polyhedron in the α-type structure has four short Li−O distances (2.23 Å) and two long Li−O distances (2.82 Å). The Li−O distances for $LiErO_2$ at 150 and 250 K are close to those for Eu^{3+}-doped $LiYO_2$ at 77 K (*β*-type) and at 383 K (α-type) in ref 7, respectively.

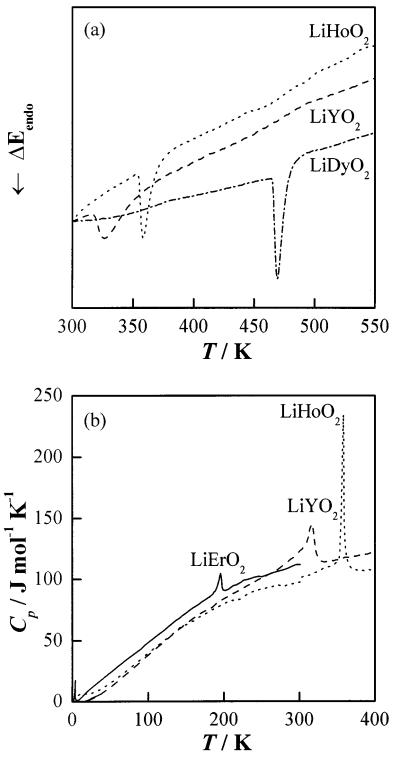

Figure 4. (a) DTA data for LiRO$_2$ with R = Y, Ho, Dy in the temperature range of 300−550 K. (b) Specific heats for LiRO$_2$ with R = Y, Ho, Er in the temperature range of 1.8−400 K.

Structural Transitions. Figures 4 (a) and (b) show the DTA data for LiRO$_2$ with R = Y, Ho, Dy in the temperature range of 300−550 K and the specific heat of LiRO$_2$ with R = Y, Ho, Er in the temperature range of 1.8−400 K, respectively. The endothermic peaks in the DTA data during heating, which are attributable to the structural transition from the β-type structure to the α-type structure, were observed at 325 K for LiYO$_2$, at 360 K for LiHoO$_2$, and at 475 K for LiDyO$_2$. The specific heat during cooling shows a peak corresponding to the first-order transitions from the α-type structure to the β-type structure at 196 K for LiErO$_2$, at 320 K for LiDyO$_2$, and at 360 K for LiHoO$_2$. In the specific heat of LiErO$_2$, one more peak due to magnetic transition is observed at 3.9 K. Figure 5 shows the plots of structural transition vs the R^{3+} ionic radius. The transition temperature increases linearly with the ionic radius of the R^{3+} ion. According to this trend, the Tm compound is expected to transform from the α-type to the β-type structure below 100 K, but the specific heat for LiTmO$_2$ shows no thermal anomaly due to a first-order transition in the temperature range of 1.8−300 K. This result is consistent with the result of the low-temperature X-ray measurements for LiTmO$_2$.

Magnetic Susceptibilities. The temperature dependence of the magnetic susceptibilities (χ) for all the LiRO$_2$ compounds except for the nonmagnetic compounds with R = Y, La, and Lu were measured in the temperature range of 1.8−300 K (1.8−400 K for LiHoO$_2$). Among the LiRO$_2$ compounds, the Ce, Pr, Nd, Eu, Tb, Ho, Tm, and Yb compounds are paramagnetic down to 1.8 K, while the Sm, Gd, Dy, and Er compounds show antiferromagnetic transitions at 2.0−4.2 K. Figure 6a,b shows the temperature dependence of the reciprocal magnetic susceptibilities of LiGdO$_2$ and LiYbO$_2$. The

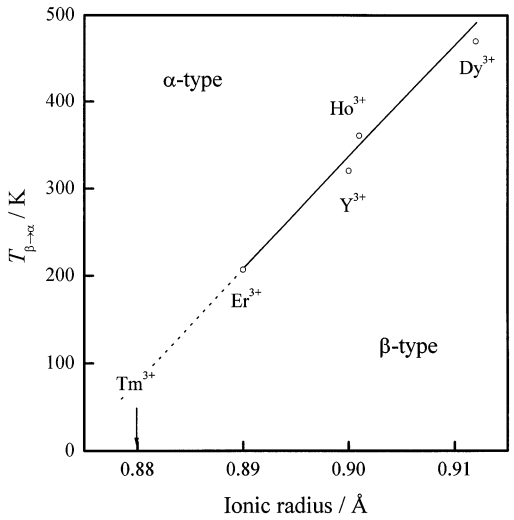

Figure 5. Structural transition temperature vs the R^{3+} ionic radius plots.

reciprocal susceptibilities of LiYbO$_2$ exhibit the Curie−Weiss behavior between 150 and 300 K but deviate from the Curie−Weiss law below 150 K, while those of LiGdO$_2$ obey the Curie−Weiss law above 5 K. The Gd^{3+} ion has the $^8S_{7/2}$ ground state without the orbital momentum, so the crystal field does not affect the susceptibility of the Gd^{3+} ions. On the other hand, the $^2F_{7/2}$ ground state of the Yb^{3+} ion should be split into four doublets in the tetragonal symmetry. The large deviation from the Curie−Weiss law below 150 K is attributable to this crystal field effect on the Yb^{3+} ion. Figure 6c,d shows the temperature dependence of the reciprocal magnetic susceptibilities of LiHoO$_2$ and LiErO$_2$. Their reciprocal magnetic susceptibilities obey the Curie−Weiss law above 50 K, except for the neighborhoods of the structural transition temperatures. Detailed reciprocal susceptibilities of LiHoO$_2$ above 340 K are shown in the inset of Figure 6c, indicating a thermal hysteresis in the susceptibility between 350 and 360 K. This experimental result is in accordance with the results by the DTA and specific heat measurements (see Figure 4), i.e., LiHoO$_2$ shows a crystallographic transformation at 360 K. The inset of Figure 6d depicts the first derivative of the reciprocal magnetic susceptibility of LiErO$_2$ in the neighborhood of 200 K. It also shows the first-order transition of LiErO$_2$ at this temperature. The magnetic susceptibility of all the LiRO$_2$ compounds, except for LiSmO$_2$ and LiEuO$_2$, obeys the Curie−Weiss law above at least 150 K. Table 4 lists the effective magnetic moments (μ_{eff}) obtained by the Curie−Weiss law fitting to the $\chi^{-1}-T$ plot. The obtained moments agree with the theoretical magnetic moments of free R^{3+} ions.

For LiSmO$_2$ and LiEuO$_2$, the spacings of the multiplet levels for the R ions are not large compared to k_BT, so the excited states should take into consideration the magnetic susceptibility. Figure 7a,b shows the temperature dependence of the magnetic susceptibilities for LiSmO$_2$ and LiEuO$_2$, respectively. The susceptibility plateau of LiEuO$_2$ below 100 K in Figure 7b is attributed to the temperature-independent term of the Van Vleck formula by the population of the nonmagnetic ground state ($^7F_0$). Considering the contribution of the excited states ^7F_J (J = 1, 2, ···, 6), the molar magnetic

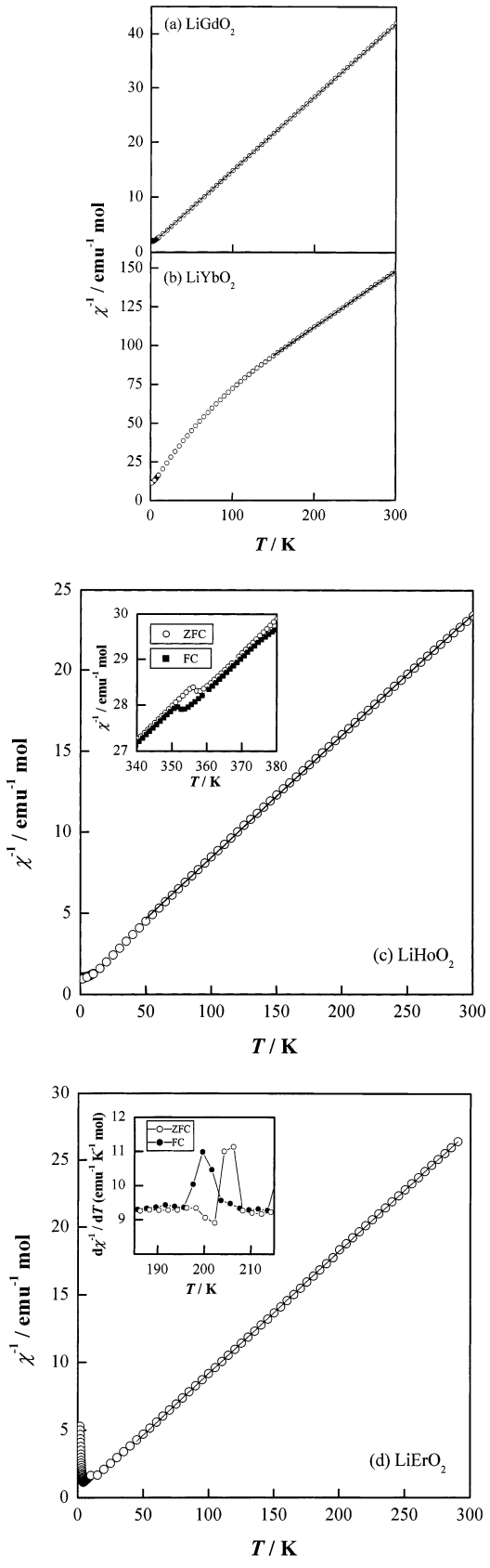

Figure 6. Temperature dependence of the reciprocal magnetic susceptibilities of (a) $LiGdO_2$, (b) $LiYbO_2$, (c) $LiHoO_2$, and (d) $LiErO_2$. The inset of Figure 6c shows the reciprocal magnetic susceptibilities in the temperature range between 340 and 380 K. The inset of Figure 6d shows the first derivative of the reciprocal magnetic susceptibilities in the temperature range between 340 and 380 K.

Table 4. Structural and Magnetic Properties of Li*R*O_2

			μ_{eff}	
R	structure	magnetic properties	obs. (μ_B)	cal. (μ_B)
Sc	α-type			
Lu	α-type			
Yb	α-type	antiferro T_N < 1.8 K	4.65	4.54
Tm	α-type	para	7.45	7.55
Er	$\beta \rightarrow$ α-type (205 K)	antiferro T_N = 4.2 K	9.38	9.59
Y	$\beta \rightarrow$ α-type (320 K)			
Ho	$\beta \rightarrow$ α-type (360 K)	para	10.30	10.58
Dy	$\beta \rightarrow$ α-type (475 K)	antiferro T_N = 3.0 K	10.03	10.63
Tb	β-type	para	9.63	9.72
	γ-type	para	9.35	9.72
Gd	γ-type	antiferro T_N = 2.5 K	7.68	7.94
Eu	γ-type	para	3.35[a]	3.40[b]
Sm	δ-type	antiferro T_N = 2.0 K	1.49[a]	1.55[b]
Nd	δ-type	antiferro T_N < 1.8 K	3.44	3.62
Pr	δ-type	para	3.56	3.58

[a] Observed values at room temperature. [b] Calculated values by Van Vleck, ref 13.

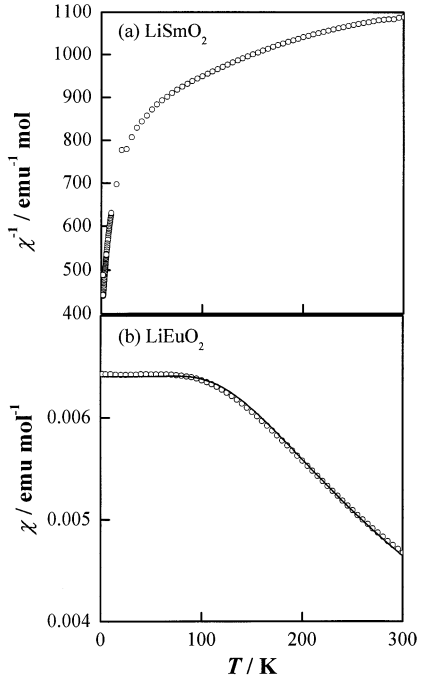

Figure 7. Temperature dependence of the magnetic susceptibilities for (a) $LiSmO_2$ and (b) $LiEuO_2$. The solid line in (b) is the calculation results by eq 2 (see text).

susceptibility for Eu^{3+} can be written by the following equation:[13]

$$\chi(Eu^{3+}) = [N_A\mu_B{}^2/3k_B]/[\gamma T]\{[24 + (13.5\gamma - 1.5)e^{-\gamma} + (67.5\gamma - 2.5)e^{-3\gamma} + (189\gamma - 3.5)e^{-6\gamma} + \cdots]/[1 + 3e^{-\gamma} + 5e^{-3\gamma} + 7e^{-6\gamma} + \cdots]\} \quad (2)$$

where $\gamma = \lambda/k_BT$ is 1/21 of the ratio of the overall multiplet width to k_BT. By fitting this equation to the experimental magnetic susceptibility, the spin−orbit coupling constant, λ, is calculated to be 327.2(5) cm^{-1}. This value agrees well with the value in other oxides containing Eu^{3+}, for example, 332 cm^{-1} for Ba_2EuTaO_6[14] and 339 cm^{-1} for Ba_2EuNbO_6.[15]

(13) Van Vleck, J. H. *The Theory of Electric and Magnetic Susceptibilities;* Clarendon: Oxford, 1932.
(14) Doi, Y.; Hinatsu, Y. *J. Phys: Condens. Matter* **2001**, *13*, 4191.

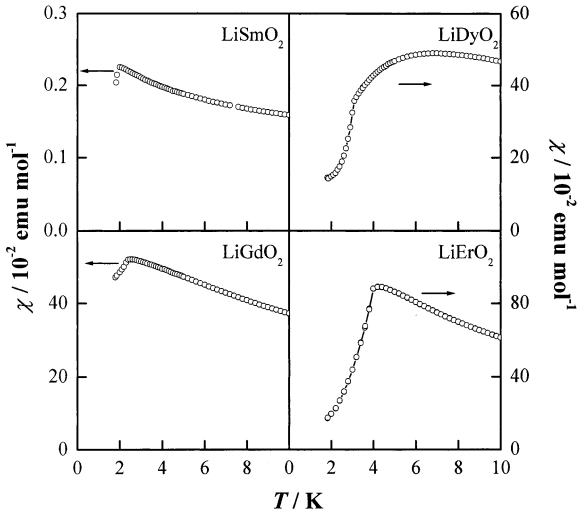

Figure 8. The low-temperature susceptibility for LiRO_2 with Sm, Gd, Dy, and Er.

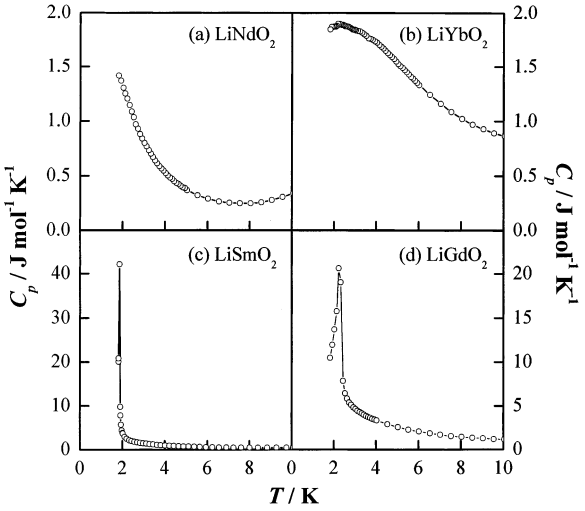

Figure 9. Temperature dependence of the specific heats for (a) $LiNdO_2$, (b) $LiYbO_2$, (c) $LiSmO_2$, and (d) $LiGdO_2$.

Magnetic Orderings in the LiRO_2 Series. Figure 8 shows the low-temperature susceptibility for LiRO_2 with Sm, Gd, Dy, and Er. A peak in the magnetic susceptibility is observed at 2.0 K for $LiSmO_2$, at 2.5 K for $LiGdO_2$, and at 4.2 K for $LiErO_2$. The susceptibility of $LiDyO_2$ shows a broad maximum at around 7 K and drops abruptly below 3.1 K. For all the LiRO_2 compounds, no divergence between the ZFC and FC susceptibilities is observed. These magnetic anomalies are attributable to the antiferromagnetic orderings of the R^{3+} moments.

Figure 9a,b shows the temperature dependence of the specific heat (C_p) of $LiNdO_2$ and $LiYbO_2$ in a low-temperature region, respectively. The specific heat of $LiNdO_2$ increases with decreasing temperatures below 7.5 K. The specific heat of $LiYbO_2$ has a broad maximum at 2.2 K. The ground states, $^4I_{9/2}$ for the Nd^{3+} ion and $^2F_{7/2}$ for the Yb^{3+} ion, are expected to split into five doublets in the monoclinic symmetry, C_2, and four doublets in the tetragonal symmetry, D_{2d}, respectively. Thus, the anomalies in their specific heat at low temperatures are attributed to a magnetic transition or a Schottky-like anomaly that occurred by a low-lying Kramers' doublet.

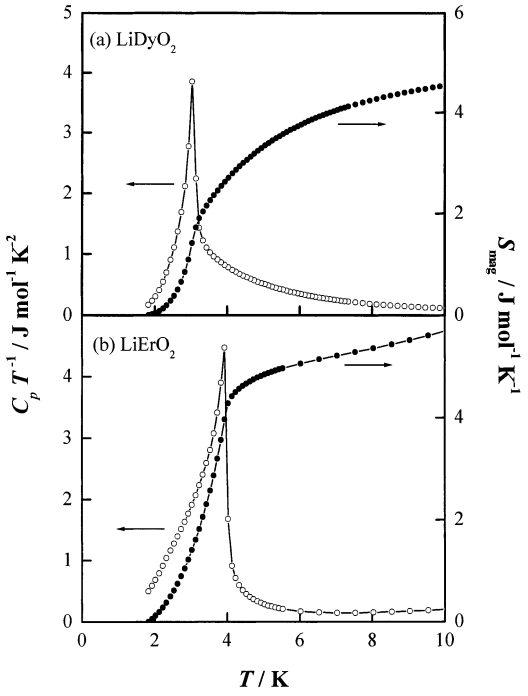

Figure 10. The C_pT^{-1}-T curve and the S_{mag}-T curve for (a) $LiDyO_2$, and (b) $LiErO_2$.

Figure 9c,d shows the temperature dependence of the specific heats for $LiSmO_2$ and $LiGdO_2$, respectively. The C_p-T curves exhibit a sharp anomaly, which corresponds to the antiferromagnetic transition in their magnetic susceptibilities at 1.9 K for $LiSmO_2$ and at 2.2 K for $LiGdO_2$. The Sm^{3+} and Gd^{3+} ions have the $^6H_{5/2}$ and $^8S_{7/2}$ ground states, respectively. The ground state of Gd^{3+} is not affected by the crystal field and the eightfold degeneracy remains, while the ground state of Sm^{3+} is expected to split into three doublets in the monoclinic symmetry, C_2. However, the degeneracy of the ground multiplets for Sm^{3+} and Gd^{3+} is not determined, because we could not estimate the magnetic entropy (S_{mag}) below 1.8 K.

Figure 10 shows the $C_pT^{-1}-T$ curve for $LiDyO_2$ and for $LiErO_2$. Both of the curves show a λ-type anomaly at 3.0 K for $LiDyO_2$ and 3.9K for $LiErO_2$, which is consistent with the results of magnetic susceptibility measurements (see Figure 8). Their $S_{mag}-T$ curves are calculated from the temperature dependence of C_p on the assumption that the lattice contribution (C_{lat}) to the total, C_p, is negligible below 10 K. They are shown in the same figure. From the $S_{mag}-T$ curve of $LiErO_2$, the magnetic entropy change at 6 K is estimated to be 5.05 J mol^{-1} K^{-1}, and it is close to R ln 2 = 5.76 J mol^{-1} K^{-1}. This result indicates that the ground multiplet of Er^{3+} is a Kramers' doublet. For the $C_pT^{-1}-T$ curve of $LiDyO_2$, C_pT^{-1} has a tail of a magnetic specific heat above the Néel temperature (~3 K) and the feature of the magnetic anomaly differs from that of $LiErO_2$. For $LiDyO_2$, S_{mag} is 1.7 J mol^{-1} K^{-1} at 3.0 K, which is less than half of R ln 2, and even a value of 4.55 J mol^{-1} K^{-1} at 10 K is smaller than R ln 2. The results of the magnetic susceptibility and specific-heat measurements for $LiDyO_2$ suggest that a short-range orderings of the

(15) Henmi, K.; Hinatsu, Y. *J. Solid State Chem.* **1999**, *148*, 353.

Dy^{3+} magnetic moments begin above 10 K and a long-range antiferromagnetic ordering occurs at 3.0 K.

Conclusion

Table 4 summarizes the structural and magnetic properties of $LiRO_2$ prepared in this study. We succeeded in preparing the β-$LiTbO_2$. The Er, Y, Ho, and Dy compounds transform from the β-type to the α-type structure at 205, 320, 360, and 475 K, respectively. The temperature of the structural transition increases with increasing the ionic radius of the R^{3+} ion. The Nd, Sm, Gd, Dy, Er, and Yb compounds show an antiferromagnetic transition at low temperatures. The magnetic behavior of $LiDyO_2$ suggests an existence of short-range magnetic orderings.

CM010728U